PERGAMON

International Journal of Heat and Mass Transfer 42 (1999) 775–788

International Journal of HEAT and MASS TRANSFER

Melting of a subcooled mixed powder bed with constant heat flux heating

Yuwen Zhang, Amir Faghri*

Department of Mechanical Engineering, University of Connecticut, 191 Auditorium Road, Storrs, CT 06269-3139, U.S.A.

Received 24 November 1997; in final form 17 July 1998

Abstract

Melting of a subcooled powder bed that contains a mixture of two powders with significantly different melting points was analytically investigated. The effect of density change on the melting process was taken into account in the physical model. The temperature distributions in the liquid and solid phases were, respectively, obtained by an exact solution and an integral approximate solution, while the effect of the unsintered powder porosity on the liquid phase shrinkage during the melting process was investigated. This effect paves the way to simulation of the complication and complex 3-D selective laser sintering (SLS) process. © 1998 Elsevier Science Ltd. All rights reserved.

Nomenclature

c_p specific heat [W kg^{-1} °C^{-1}]
g gravity acceleration [m s^{-2}]
h_{sl} latent heat of melting or solidifcation [J kg^{-1}]
k thermal conductivity [W m^{-1} °C^{-1}]
K_g dimensional thermal conductivity of gas(es)
K_s dimensionless effective thermal conductivity of unsintered powder
p pressure [Pa]
q_{in} heat flux [W m^{-2}]
s solid–liquid interface location [m]
s_0 location of liquid surface [m]
S dimensionless solid–liquid interface location
S_0 dimensionless location of liquid surface
Sc subcooling parameter
t time [s]
T temperature [°C]
V volume [m^3]
w velocity of liquid phase [m s^{-1}]
W dimensionless velocity of the liquid phase
z coordinate [m]
Z dimensionless coordinate.

Greek symbols
α thermal diffusivity [m^2 s^{-1}]
δ thickness of thermal layer [m]
Δ dimensionless thickness of thermal layer
ε volume fraction of gas(es) (porosity for unsintered powder)
θ dimensionless temperature
ρ density [kg m^{-3}]
τ dimensionless time
ϕ volume fraction of the low melting point powder in the powder mixture.

Subscripts
g gas(es)
H high melting point powder
i initial
l liquid phase (mixture of low melting point metal liquid and high melting point powder solid)
L low melting point powder
m melting point
p resolidified part
s unsintered solid (mixture of two solid powders).

1. Introduction

Solid Freeform Fabrication (SFF) with Selective Laser Sintering (SLS) is an emerging technology in which 3-D parts are built using CAD data [1]. SLS of metal powder involves fabrication of near full density objects from powder via melting and resolidification induced by a directed

* Corresponding author

PII: S0017–9310(98)00231–2

laser beam (generally CO_2 or YAG). It is very important to develop a powerful heat transfer model to predict the temperature distribution in the SLS process since it has significant effect on the quality of the final product. Some existing heat transfer models concerning SLS [2, 3] only consider pure conduction in the powder bed which is obviously limited and oversimplified. Kandis and Bergman [4] presented an experimental investigation and numerical prediction of the sintering of the polymer powder, which has little crystallinity and a nearly zero latent heat of fusion. For metal powder, the powder melts after absorbing a large amount of heat from the laser beam and then releases the heat during resolidification to form the mechanical parts. The melting and resolidification processes will have significant effect on the temperature distribution, residual stress and the final quality of the parts. It is not difficult to imagine that the neglecting of such an important effect would result in significant error in thermal modeling. Melting in the SLS process is significantly different from the normal melting phenomenon since the volume fraction of the gas(es) in the powder decreases from a large value, up to 0.5, to nearly zero after melting. Thus, significant density change accompanies the melting process.

Melting and solidification phenomena have been intensively investigated during the past three decades and detailed reviews concerning the fundamental aspects and applications can be found in the existing literature [5, 6]. The change of density of the Phase Change Materials (PCMs) is usually associated with the melting and solidifcation process. This density change may occur at the phase transition or may be caused by dependence of the liquid density on the temperature. Most scientists have ignored the density change caused by phase transition. For liquid density variation with temperature, it has usually been assumed that the liquid is incompressible and accounts for the effect of liquid density change on the buoyancy force only if natural convection in the liquid is considered.

The effect of density change during the solid–liquid phase change process has been considered by a few scientists. Solidification of a 1-D semi-infinite body with density change in phase transition has been solved using the similarity solution by Eckert and Drake [7], Crank [8] and Carslaw and Jaeger [9]. Charach and Zarmi [10] solved planar solidifcation in a vertical finite slab cooled from below with the effect of density change taken into account. The problem was reduced to that without density change by use of the Rubinstein transformation to immobilize the interface. Conti [11] solved a similar problem numerically by considering the pressure dependence effect of the freezing point. The Clapeyron equation was employed to determine the variation of the melting point with change of pressure. Shrinkage formation due to density change during the solidifcation process in a 2-D cavity was investigated numerically by Kim and Ro [12]. They concluded that the density change played a more important role than convection in the solidifcation process.

In order to understand the melting dynamics of spherical particles, Shah [13] experimentally investigated melting of a single column of solder particle (eutectic Sn–Pb) held vertically inside a glass tube. A compressive load acts on the top of the column and the bottom of the surface was heated by a heater at a specified temperature. The problem is also formulated using an enthalpy model and solved using a finite difference method. It should be noted that melting of the powder bed during SLS occurs under the boundary condition of specified heat flux instead of specified temperature. This means that the similarity solution method employed by refs [7–10] cannot be applied. Moreover, for SLS of a metal powder, Manzur et al. [14] and Bunnell [15] proposed to use a powder mixture which contained two powders of significantly different melting points. Only the low melting point powder will be melted and resolidified during the SLS process and the high melting point powder remains solid during the whole process. Particles of the high melting point powder move with the liquid of low melting point and hence a fully densified part can be formed. Significant density change occurs during this process. The complete modeling of SLS involves a two phase (solid–gas) to three phase (solid, liquid and gas). Mughal and Plumb [16, 17] have modeled a similar system, but it was limited to 1-D response and the high melting point powder was assumed to be fixed in space after the low melting point powder is melted. Since they had different applications, heat was induced by internal heat source. In this investigation, melting of a powder bed containing a powder mixture under a boundary condition of the second kind will be solved using a semi-exact solution. The effect of liquid motion will also be investigated.

2. Thermal properties

Thermal property evaluation is very important in the prediction of the melting process of the powder bed. It should be noted that there are three components in the powder bed: low melting point powder, high melting point powder and gas(es). For the sake of simplicity, it is assumed that the thermal properties of the low melting point powder are the same for both liquid and solid phase.

After the powder bed is molten, in an ideal situation, all of the gas(es) are driven from the powder bed by shrinkage so that fully densified parts can be formed after resolidification. Therefore, the thermal properties of the ideal liquid pool or resolidified part can be expressed as

$$\rho_p = \phi\rho_L + (1-\phi)\rho_H \quad (1)$$

$$(\rho c_p)_p = \phi\rho_L c_{pL} + (1-\phi)\rho_H c_{pH} \quad (2)$$

$$k_p = \phi k_L + (1-\phi)k_H. \quad (3)$$

Before melting, gas(es) exist in the pore space between particles of the powder. It is straightforward to express the density and heat capacity of the unsintered powder bed as:

$$\rho_s = (1-\varepsilon_s)[\phi\rho_L + (1-\phi)\rho_H] + \varepsilon_s\rho_g = (1-\varepsilon_s)\rho_p + \varepsilon_s\rho_g$$

$$(\rho c_p)_s = (1-\varepsilon_s)[\phi\rho_L c_{pL} + (1-\phi)\rho_H c_{pH}] + \varepsilon_s(\rho c_p)_g = (1-\varepsilon_s)(\rho c_p)_p + \varepsilon_s(\rho c_p)_g$$

where ε_s is the volume fraction of the gas(es) in the unsintered powder bed. It coincides with porosity for the unsintered powder bed, i.e.

$$\varepsilon_s = \frac{V_g}{V_g + V_L + V_H}$$

ϕ is the volume percentage of the low melting powder in the powder mixture, i.e.

$$\phi = \frac{V_L}{V_L + V_H}.$$

The order of magnitude of the typical metal powder, such as aluminum and iron and gas(es) thermal properties are as follows

$$\rho_L \sim \rho_H \sim 10^3 \text{ kg m}^{-3}, \quad \rho_g \sim 1 \text{ kg m}^{-3}$$

$$k_L \sim k_H \sim 10^2 \text{ W m}^{-1}\text{ K}^{-1}, \quad k_g \sim 10^{-2} \text{ W m}^{-1}\text{ K}^{-1}$$

$$c_{pL} \sim c_{pH} \sim 10^2 \text{ J kg}^{-1}\text{ K}^{-1}, \quad c_{pg} \sim 1 \text{ J kg}^{-1}\text{ K}^{-1}.$$

Thus, the contributions of the gas(es) to the density and heat capacity of the powder bed are negligible. The thermal properties of the powder bed before sintering are, therefore, expressed as

$$\rho_s = (1-\varepsilon_s)\rho_p = (1-\varepsilon_s)[\phi\rho_L + (1-\phi)\rho_H] \quad (4)$$

$$(\rho c_p)_s = (1-\varepsilon_s)(\rho c_p)_p = (1-\varepsilon_s)[\phi\rho_L c_{pL} + (1-\phi)\rho_H c_{pH}]. \quad (5)$$

In reality, the gas(es) in the powder bed may not be driven out completely and the gas(es) may exist in the liquid phase as well. In this case, the volume fraction of the gas(es) in the liquid pool is not zero and therefore, the density and thermal capacity of the liquid phase is expressed in the following generalized form

$$\rho_l = (1-\varepsilon_l)\rho_p = (1-\varepsilon_l)[\phi\rho_L + (1-\phi)\rho_H] \quad (6)$$

$$(\rho c_p)_l = (1-\varepsilon_l)(\rho c_p)_p = (1-\varepsilon_l)[\phi\rho_L c_{pL} + (1-\phi)\rho_H c_{pH}] \quad (7)$$

where ε_l is the volume fraction of the gas(es) in the liquid phase of the powder bed, which is a mixture of low melting metal liquid and high melting point powder particles, i.e.

$$\varepsilon_l = \frac{V_g}{V_g + V_L + V_H}.$$

It is noted that this is not the porosity for the liquid phase of the powder bed.

Specification of thermal conductivity of the powder bed before sintering is very complicated. The effective thermal conductivity of the powder depends on the arrangement of the particles in the powder bed and the order of magnitude of the gas(es) and the particle. The contact between the particles also plays a significant role on the value of the thermal conductivity. Shah [13] used a thermal conductivity correlation accounting for the compressive force acting on the top of the column. For the case of large thermal conductivity ratio, k_p/k_g, the empirical correlation proposed by Hadley [18] appears to be the best correlation since it agrees with the experimental data very well. Therefore, the effective thermal conductivity of the powder bed before sintering will be calculated by the following correlation [18]:

$$\frac{k_s}{k_g} = (1-\alpha_0)\frac{\varepsilon_s f_0 + k_p/k_g(1-\varepsilon_s f_0)}{1-\varepsilon_s(1-f_0)+k_p/k_g\varepsilon_s(1-f_0)} + \alpha_0\frac{2(k_p/k_g)^2(1-\varepsilon_s)+(1+2\varepsilon_s)k_p/k_g}{(2+\varepsilon_s)k_p/k_g+1-\varepsilon_s} \quad (8)$$

where

$$f_0 = 0.8 + 0.1\varepsilon_s \quad (8a)$$

$$\log\alpha_0 = \begin{cases} -4.898\varepsilon_s & 0 \leqslant \varepsilon_s \leqslant 0.0827 \\ -0.405 - 3.154(\varepsilon_s - 0.0827) & 0.0827 \leqslant \varepsilon_s \leqslant 0.298. \\ -1.084 - 6.778(\varepsilon_s - 0.298) & 0.298 \leqslant \varepsilon_s \leqslant 0.580 \end{cases} \quad (8b)$$

When the low melting point powder is molten, the contact area between the two powders is significantly increased and therefore, it is expected that the effective thermal conductivity of the low melting point liquid metal and high melting point powder mixture is higher than that before melting. The thermal conductivity of liquid is, therefore, calculated by using a parallel arrangement, i.e.

$$k_l = (1-\varepsilon_l)k_p. \quad (9)$$

Obviously, when the gas(es) are completely driven out, the effective thermal conductivity of the liquid given by equation (9) becomes k_p, which is defined by equation (3).

In addition, we have the following relation

$$\alpha_l = \frac{k_l}{(\rho c_p)_l} = \frac{k_p}{(\rho c_p)_p} = \alpha_p.$$

The thermal properties of the solid and liquid have the following relation

$$\frac{(\rho c_p)_s}{\rho_s} = \frac{(\varepsilon c_p)_l}{\rho_l} = \frac{(\rho c_p)_0}{\rho_0} = c_p$$

i.e.

$c_{ps} = c_{pl} = c_p$.

3. Physical model

3.1. Governing equations

The physical model of the problem is shown in Fig. 1. A powder bed, which contains two powders with significantly different melting points, with a uniform initial temperature below the melting point of the low melting point powder, T_m, is in a half space, $z > 0$. At time $t = 0$, a constant heat flux, q_{in}, is suddenly applied to the surface of the semi-infinite body. Since the initial temperature of the powder bed is below the melting point of the low melting point powder, melting of the low melting point powder will not occur simultaneously with the beginning of the heating. Only after a finite period of time, in which the surface temperature of the powder reaches the melting point of the low melting point powder, will the melting start. This feature is distinct from the melting of a subcooled semi-infinite body with a boundary condition of the first kind, in which the melting starts simultaneously with heating. It should be noted that the temperature of the powder bed will never reach the melting point of the high melting point powder during the entire process and therefore, only low melting point powder melts.

The problem can be divided into two subproblems. One is the heat conduction during pre-heating and the other is the melting process. An integral approximate method [19] and a semi-exact method [20] will be, respectively, employed to solve these two subproblems.

At the start of heating, no melting occurs and the problem is a pure conduction problem with boundary conditions of the second kind. This problem is solved using an integral approximate method by assuming a second-degree polynomial temperature profile. The highest temperature of the semi-infinite body occurs at its surface ($z = 0$) and can be expressed as

$$T_0(t) = T_i + \frac{q_{in}\sqrt{6\alpha_s t}}{2k_s}. \tag{10}$$

Melting occurs when the surface temperature reaches the melting point, T_m, of the powder with low melting point and the duration of pre-heating can be calculated from

$$t_m = \frac{2k_s^2(T_m - T_i)^2}{3\alpha_s q_{in}^2}. \tag{11}$$

The corresponding thermal layer thickness and temperature distribution at time t_m are found by

$$\delta_m = \frac{2k_s(T_m - T_i)}{q_{in}} \tag{12}$$

$$T_s(z, t_m) = T_i + (T_m - T_i)\left(1 - \frac{z}{\delta_m}\right)^2. \tag{13}$$

The melting process will start at time $t = t_m$. It should be noted that the surface of the powder bed moves downward with volume shrinkage during the melting of the powder bed. Since the powder bed goes through a very rapid melting and resolidification in a real SLS process, the time that the liquid presents at any points of the powder bed is very short (typically in the order of 1 s). Therefore, it is expected that the effect of liquid flow caused by the capillary and gravity forces is negligible. In addition, the following assumptions are made:

(1) Liquid phase is assumed to be incompressible.
(2) The melting point of low melting point powder is not affected by pressure.

For a fixed coordinate system, z, the governing equations and boundary conditions for the liquid phase are expressed as [10]:

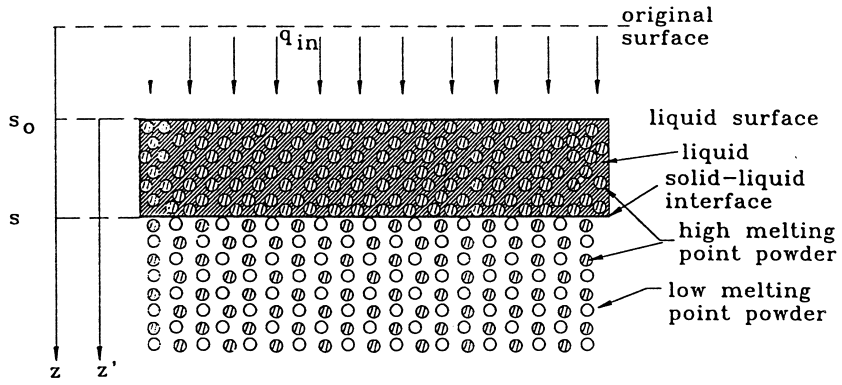

Fig. 1. Melting in a powder bed containing two powders with different melting points.

$$\frac{\partial w}{\partial z}=0,\quad s_0<z<s(t),\quad t>t_m \tag{14}$$

$$\rho_l\frac{\partial w}{\partial t}=-\frac{\partial p}{\partial z}+\rho_l g,\quad s_0<z<s(t),\quad t>t_m \tag{15}$$

$$\alpha_l\frac{\partial^2 T_l}{\partial z^2}=\frac{\partial T_l}{\partial t}+w\frac{\partial T_l}{\partial z},\quad s_0<z<s(t),\quad t>t_m \tag{16}$$

$$w=\frac{ds_0}{dt},\quad z=s_0,\quad t>t_m \tag{17}$$

$$\frac{\partial T_l(z,t)}{\partial z}=-\frac{1}{k_l}q_{in},\quad z=s_0,\quad t>t_m. \tag{18}$$

Since the liquid phase is assumed to be incompressible, the entire liquid moves with a velocity, w and the viscosity of the liquid has no effect on the liquid motion.

Pure conduction heat transfer occurs in the solid in the fixed coordinate system, z. The governing equation and the corresponding boundary conditions in the solid phase are

$$\alpha_s\frac{\partial^2 T_s}{\partial z^2}=\frac{\partial T_s}{\partial t},\quad s(t)<z<\infty,\quad t>t_m \tag{19}$$

$$T_s(z,t)\to T_i,\quad z\to\infty,\quad t>t_m \tag{20}$$

$$T_s(z,t)=T_i+(T_m-T_i)\left(1-\frac{z}{\delta_m}\right)^2,\quad z>0,\quad t=t_m. \tag{21}$$

The conservation of mass at the solid–liquid interface gives us

$$\rho_l w=(\rho_l-\rho_s)\frac{ds}{dt}. \tag{22}$$

Substituting equations (4) and (6) into equation (22) yields

$$w=\frac{\varepsilon_s-\varepsilon_l}{1-\varepsilon_l}\frac{ds}{dt} \tag{23}$$

and the energy balance at the solid–liquid interface is

$$k_s\frac{\partial T_s}{\partial z}-k_l\frac{\partial T_l}{\partial z}=(1-\varepsilon_s)\phi\rho_L h_{sl}\frac{ds}{dt},\quad z=s(t),\quad t>t_m. \tag{24}$$

The temperature at the interface should satisfy

$$T_l(z,t)=T_s(z,t)=T_m,\quad z=s(t),\quad t>t_m. \tag{25}$$

The solution of equation (15) can be obtained by substituting equation (23) and integrating. The result is

$$p=p_{atm}+\rho_l\left[g-\frac{\varepsilon_s-\varepsilon_l}{1-\varepsilon_l}\frac{d^2 s}{dt^2}\right](z-s_0). \tag{26}$$

The pressure difference in the liquid phase is small since the second term of the right-hand side of equation (26) is expected to be small. Therefore, the dependence of the melting point on the pressure is not taken into account.

3.2. Scale analysis

In order to examine the suitability of neglecting the convection term in equation (16), a scale analysis is performed.

A scale analysis of equation (16) is expressed as

$$T_l\sim\frac{s-s_0}{k_l}q_{in},\quad z\sim s,\quad t\sim t,\quad w\sim\frac{\varepsilon_s-\varepsilon_l}{1-\varepsilon_l}\frac{s}{t}.$$

Applying the above to equation (16) yields

$$\alpha_l\frac{\frac{s-s_0}{k_l}q_{in}}{s^2}\sim\frac{\frac{s-s_0}{k_l}q_{in}}{t}+\frac{\varepsilon_s-\varepsilon_l}{1-\varepsilon_l}\frac{s}{t}\frac{\frac{s-s_0}{k_l}q_{in}}{s^2}$$

i.e.

$$1\sim\frac{s^2}{\alpha_l t}+\frac{\varepsilon_s-\varepsilon_l}{1-\varepsilon_l}\frac{s^2}{\alpha_l t}.$$

It can be seen that the order of magnitude of the second term in the right-hand side, i.e., convection term, depends on the relative density change in the melting process. In the traditional melting and freezing problem [7–11], the relative density change is very small and therefore, the velocity induced by density change is also quite small. However, for a typical laser sintering process, say, $\varepsilon_s=0.4$ and $\varepsilon_l=0$, the relative density change is 40% and therefore, the convection term is 40% of the transient term int he energy equation. This is clear evidence that neglection of the advection term in the energy equation is inappropriate and will result in significant error.

3.3. Non-dimensional governing equations

By defining the following dimensionless variables:

$$\theta_l=\frac{(\rho c_p)_p(T_l-T_m)}{\phi\rho_L h_{sl}},\quad \theta_s=\frac{(\rho c_p)_p(T_s-T_m)}{\phi\rho_L h_{sl}},$$

$$Sc=\frac{(\rho c_p)_p(T_m-T_i)}{\phi\rho_L h_{sl}}\quad Z=\frac{z}{\alpha_p\phi\rho_L h_{sl}/q_{in}},$$

$$S=\frac{s}{\alpha_p\phi\rho_L h_{sl}/q_{in}},\quad \Delta=\frac{\delta}{\alpha_p\phi\rho_L h_{sl}/q_{in}}$$

$$S_0=\frac{s_0}{\alpha_p\phi\rho_L h_{sl}/q_{in}},\quad W=(\phi\rho_L h_{sl}/q_{in})w,$$

$$\tau=\frac{\alpha_p t}{(\alpha_p\phi\rho_L h_{sl}/q_{in})^2}\quad K_s=\frac{k_s}{k_p(1-\varepsilon_s)},\quad K_g=\frac{k_g}{k_p} \tag{27}$$

the governing equations of the problem become

$$\frac{\partial^2\theta_l}{\partial Z^2}=\frac{\partial\theta_l}{\partial\tau}+W\frac{\partial\theta_l}{\partial Z},\quad S_0<Z<S(\tau),\quad \tau>\tau_m \tag{28}$$

$$W=\frac{dS_0}{d\tau},\quad Z=S_0,\quad \tau>\tau_m \tag{29}$$

$$\frac{\partial\theta_l(Z,\tau)}{\partial Z} = -\frac{1}{1-\varepsilon_l}, \quad Z = S_0, \quad \tau > \tau_m \tag{30}$$

$$K_s\frac{\partial^2\theta_s}{\partial Z^2} = \frac{\partial\theta_s}{\partial\tau}, \quad S(\tau) < Z < \infty, \quad \tau > \tau_m \tag{31}$$

$$\theta_s(Z,\tau) \to -Sc, \quad Z \to \infty, \quad \tau > \tau_m \tag{32}$$

$$W = \frac{\varepsilon_s-\varepsilon_l}{1-\varepsilon_l}\frac{dS}{d\tau} \tag{33}$$

$$\theta_s(Z,\tau) = Sc\left[\left(1-\frac{Z}{\Delta_m}\right)^2 - 1\right], \quad Z > 0, \quad \tau = \tau_m \tag{34}$$

$$K_s\frac{\partial\theta_s}{\partial Z} - \frac{1-\varepsilon_l}{1-\varepsilon_s}\frac{\partial\theta_l}{\partial Z} = \frac{dS}{d\tau}, \quad Z = S(\tau), \quad \tau > \tau_m \tag{35}$$

$$\theta_l(Z,\tau) = \theta_s(Z,\tau) = 0, \quad Z = S(\tau), \quad \tau > \tau_m \tag{36}$$

where Δ_m and τ_m can be obtained by substituting equation (27) into equations (11) and (12) for the following

$$\tau_m = \tfrac{2}{3}(1-\varepsilon_s)^2 K_s Sc^2 \tag{37}$$

$$\Delta_m = 2(1-\varepsilon_s)K_s Sc. \tag{38}$$

The dimensionless thermal conductivity, K_s, can be obtained by non-dimensionalizing equation (8), i.e.

$$K_s = K_g(1-\alpha_0)\frac{\varepsilon_s f_0 + (1-\varepsilon_s f_0)/K_g}{1-\varepsilon_s(1-f_0)+\varepsilon_s(1-f_0)/K_g} + K_g\alpha_0\frac{2(1-\varepsilon_s)/K_g^2 + (1+2\varepsilon_s)/K_g}{(2+\varepsilon_s)/K_g + 1-\varepsilon_s}. \tag{39}$$

4. Semi-exact solution

At the beginning of the melting process, the solid–liquid interface moves in the positive axial direction of z while the surface of the powder bed moves in the same direction due to shrinkage. At the same time, the thermal layer thickness will continuously increase. In the solid phase, the temperature in the range of $S(\tau) < Z < \Delta(\tau)$ is affected by the boundary condition at the surface of the semi-infinite body while the temperature in the region beyond the thermal layer thickness, Δ, is not affected and remains at $-Sc$.

Integrating equation (31) in the interval of (S,Δ) and from the definition of the thermal layer and equation (36), we can obtain the integral equation of the solid phase as

$$-K_s\left.\frac{\partial\theta_s}{\partial Z}\right|_{Z=S} = \frac{d}{d\tau}(\Theta_s + Sc\Delta) \tag{40}$$

where

$$\Theta_s = \int_S^\Delta \theta_s\, dZ. \tag{41}$$

Assuming the temperature distribution in the solid phase is a second-order polynomial function and determining the constants in the polynomial function yields

$$\theta_s(Z,\tau) = Sc\left[\left(\frac{\Delta-Z}{\Delta-S}\right)^2 - 1\right]. \tag{42}$$

Substituting equation (42) into equation (40), we get

$$\frac{6K_s}{\Delta-S} = 2\frac{dS}{d\tau} + \frac{d\Delta}{d\tau} \tag{43}$$

which describes the relationship between the location of the solid–liquid interface and the thermal layer thickness.

Since the entire liquid phase moves with velocity W, the liquid phase is static from the coordinate, Z', which moves with velocity W. The relationship between the two coordinate systems is

$$Z' = Z - \int_0^\tau W\, d\tau = Z - S_0. \tag{44}$$

The energy equation and the corresponding boundary conditions are

$$\frac{\partial^2\theta_l}{\partial Z'^2} = \frac{\partial\theta_l}{\partial\tau}, \quad 0 < Z' < S-S_0, \quad \tau > \tau_m \tag{45}$$

$$\frac{\partial\theta_l}{\partial Z'} = -\frac{1}{1-\varepsilon_l}, \quad Z' = 0, \quad \tau > \tau_m \tag{46}$$

$$\theta_l(Z',\tau) = 0, \quad Z' = S-S_0, \quad \tau > \tau_m. \tag{47}$$

The exaction solution of equations (45)–(47) is [21]

$$\theta_l(Z',\tau) = \frac{2\sqrt{\tau-\tau_m}}{1-\varepsilon_l}\left[i\,\mathrm{erfc}\left(\frac{Z'}{2\sqrt{\tau-\tau_m}}\right) - i\,\mathrm{erfc}\left(\frac{S-S_0}{2\sqrt{\tau-\tau_m}}\right)\right]. \tag{48}$$

Changing back to the Z coordinate system yields

$$\theta_l(Z,\tau) = \frac{2\sqrt{\tau-\tau_m}}{1-\varepsilon_l}\left[i\,\mathrm{erfc}\left(\frac{Z-S_0}{2\sqrt{\tau-\tau_m}}\right) - i\,\mathrm{erfc}\left(\frac{S-S_0}{2\sqrt{\tau-\tau_m}}\right)\right]. \tag{49}$$

Substituting equations (49) and (42) into equation (35), one can obtain

$$\frac{dS}{d\tau} = \frac{1}{1-\varepsilon_s}\mathrm{erfc}\left(\frac{S-S_0}{2\sqrt{\tau-\tau_m}}\right) - \frac{2K_s Sc}{\Delta-S}. \tag{50}$$

Combining equations (29) and (33) and integrating yields

$$S_0 = \frac{\varepsilon_s-\varepsilon_l}{1-\varepsilon_l}S. \tag{51}$$

Substituting equation (51) into equation (50), we get

$$\frac{dS}{d\tau} = \frac{1}{1-\varepsilon_s}\mathrm{erfc}\left[\frac{(1-\varepsilon_s)S}{2(1-\varepsilon_l)\sqrt{\tau-\tau_m}}\right] - \frac{2K_s Sc}{\Delta-S}. \tag{52}$$

Substituting equation (52) into equation (43), a differential equation of Δ is obtained.

$$\frac{d\Delta}{d\tau} = \frac{6K_s}{\Delta - S}\left(1+\frac{2}{3}Sc\right) - \frac{2}{1-\varepsilon_s}\operatorname{erfc}\left[\frac{(1-\varepsilon_s)S}{2(1-\varepsilon_l)\sqrt{\tau-\tau_m}}\right]. \tag{53}$$

The initial conditions of equation (52) and (53) are

$$S(\tau_m) = 0 \tag{54}$$

$$\Delta(\tau_m) = \Delta_m = 2(1-\varepsilon_s)K_s Sc. \tag{55}$$

Equations (52) and (53) can be easily solved by the Runge–Kutta method.

It should be noted that if $\varepsilon_s = \varepsilon_l = Sc = 0$, equation (52) is reduced to

$$\frac{dS}{d\tau} = \operatorname{erfc}\left(\frac{S}{2\sqrt{\tau}}\right) \tag{56}$$

which is identical to the result of El-Genk and Cronenberg [21].

5. Results and discussion

The powder bed surface temperature is a very important parameter. By non-dimensionalizing equation (10), the surface temperature before melting is obtained. The surface temperature after melting is obtained by substituting $Z = S_0$ into equation (49), i.e.

$$\theta_0 = \begin{cases} -Sc + \dfrac{\sqrt{6K_s\tau}}{2K_s(1-\varepsilon_s)} & \tau \leqslant \tau_m \\ \sqrt{2\tau}\left[\dfrac{1}{\sqrt{\tau}} - i\operatorname{erfc}\left(\dfrac{(1-\varepsilon_s)S}{2(1-\varepsilon_l)\sqrt{\tau-\tau_m}}\right)\right] & \tau > \tau_m \end{cases}. \tag{57}$$

The effect of the volume fraction of the gas(es) in the powder bed on the surface temperature during the melting process is shown in Fig. 2. Shrinkage of the powder bed is not taken into account in Figs 2 and 3, i.e., the volume fraction of the gas(es) of the liquid phase, ε_l and that of solid phase, ε_s, are assumed to be identical. As can be seen, the surface temperature of the powder bed is below the melting point in the very beginning and is increased gradually until reaching the melting point. The duration of pre-heating decreases with an increase of the volume fraction of the gas(es) since the effective thermal conductivity of the powder bed decreases with an increase of the volume fraction of the gas(es). Figure 3 shows the location of the solid–liquid interface corresponding to conditions of Fig. 2. It can be seen that melting occurs after the surface temperature reaches the melting point. The velocity of the solid–liquid interface is faster when the volume fraction of the gas(es) is higher. Since shrinkage is not taken into account, the surface

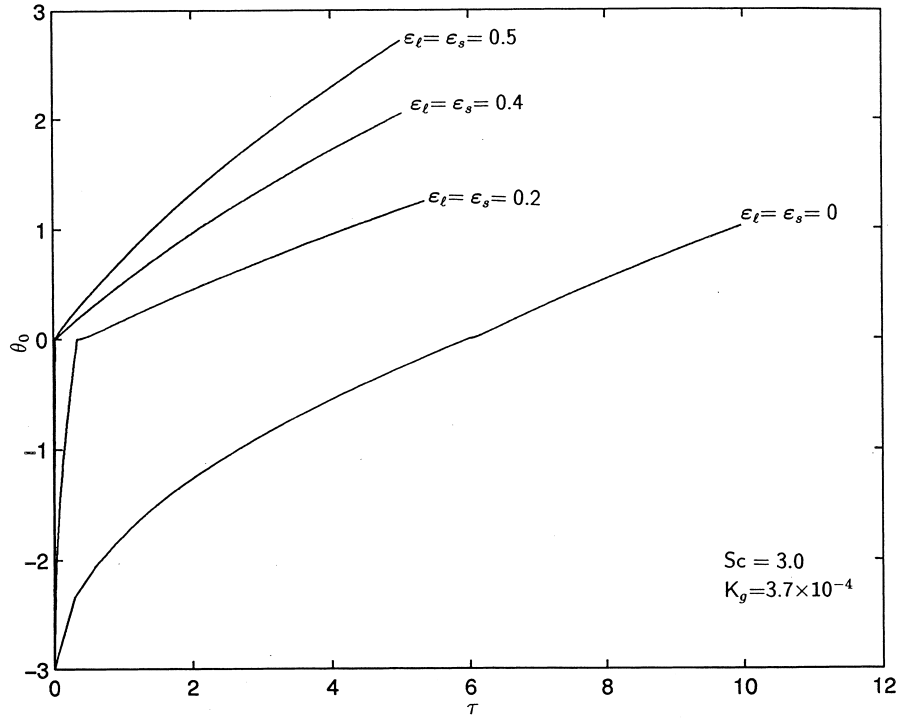

Fig. 2. Effect of porosity on the surface temperature (without shrinkage).

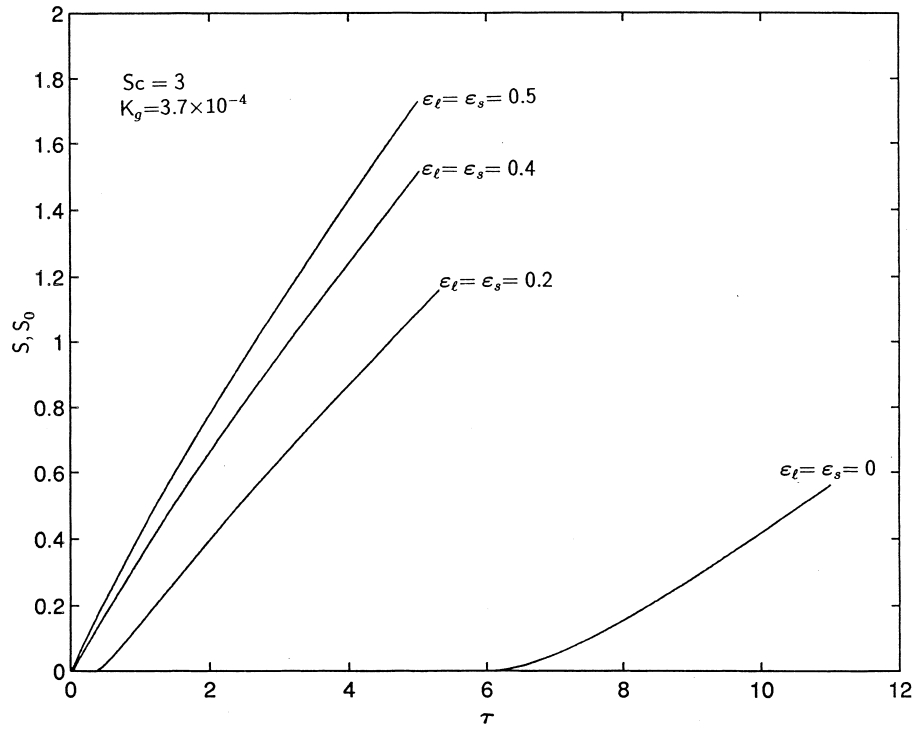

Fig. 3. Effect of porosity on the location of the solid–liquid interface (without shrinkage).

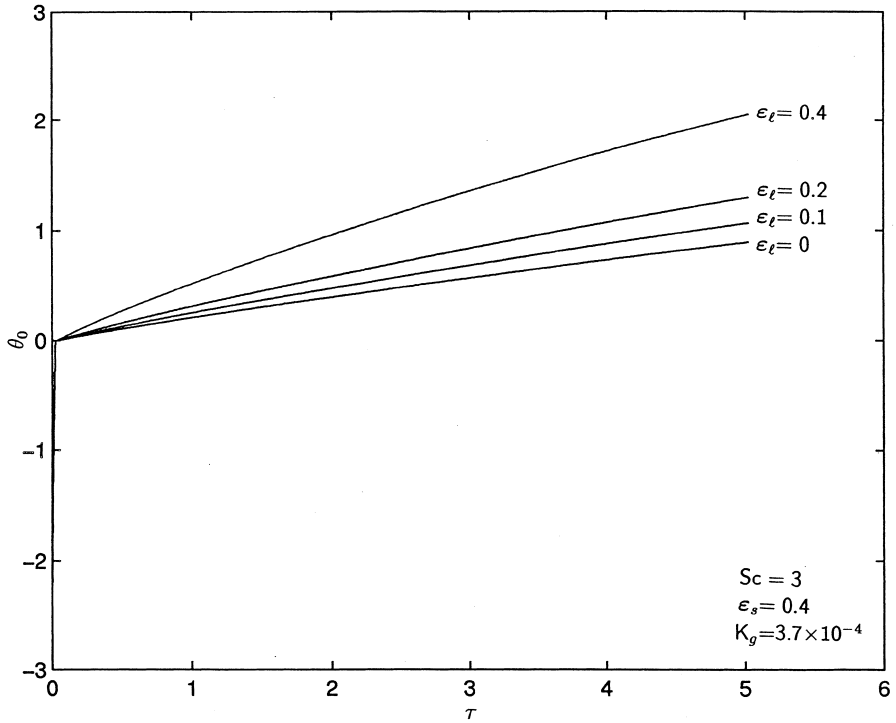

Fig. 4. Effect of porosity in the liquid phase on surface temperature.

of the powder bed stays at $S_0 = 0$ and does not move downward.

Figure 4 shows the effect of volume fraction of the gas(es) in the liquid phase on the surface temperature. The subcooling parameter and the porosity of the solid phase are fixed in order to isolate the effect of shrinkage during the melting process. It can be seen that the duration of pre-heating is the same for all cases since it only depends on the subcooling and porosity in the solid phase. The surface temperature increases with an increase of porosity in the liquid phase since a higher volume fraction of the gas(es) means lower effective thermal conductivity in the liquid phase. The locations of liquid surface and solid–liquid interface corresponding to the conditions of Fig. 4 are shown in Fig. 5. It can be seen that the densification during the melting process accelerates the melting process. The motion of the solid–liquid interface is fastest when the powder bed is fully densified upon melting. The corresponding locations of the liquid surface are also shown in Fig. 5 by a dashed line. It can be seen that the liquid surface moves downward significantly due to the shrinkage of the powder bed during the melting process. It is not difficult to imagine the error of neglecting the effect of shrinkage on the melting process.

Figure 6 shows the effect of initial subcooling of the powder bed on the surface temperature of the powder bed. From the definition of the subcooling parameter in equation (27), its value depends on the thermal properties of the powder, initial temperature of the powder bed and percentage of low melting point powder. Therefore, the subcooling parameter varies in a wide range. Figure 6 shows the surface temperature at three different initial subcooling parameters. It can be seen that the duration of pre-heating is slightly increased with an increase of the subcooling parameter. The surface temperature after melting is lower for larger initial subcooling. Figure 7 shows the effect of subcooling on the locations of liquid surface and the solid–liquid interface. As can be seen, the existence of initial subcooling reduces the velocity of the solid–liquid interface substantially. However, the relationship of the liquid surface and the solid–liquid interface is the same for different subcooling parameters since it only depends on the volume fractions of the gas(es) of the solid and liquid phase, which are the same

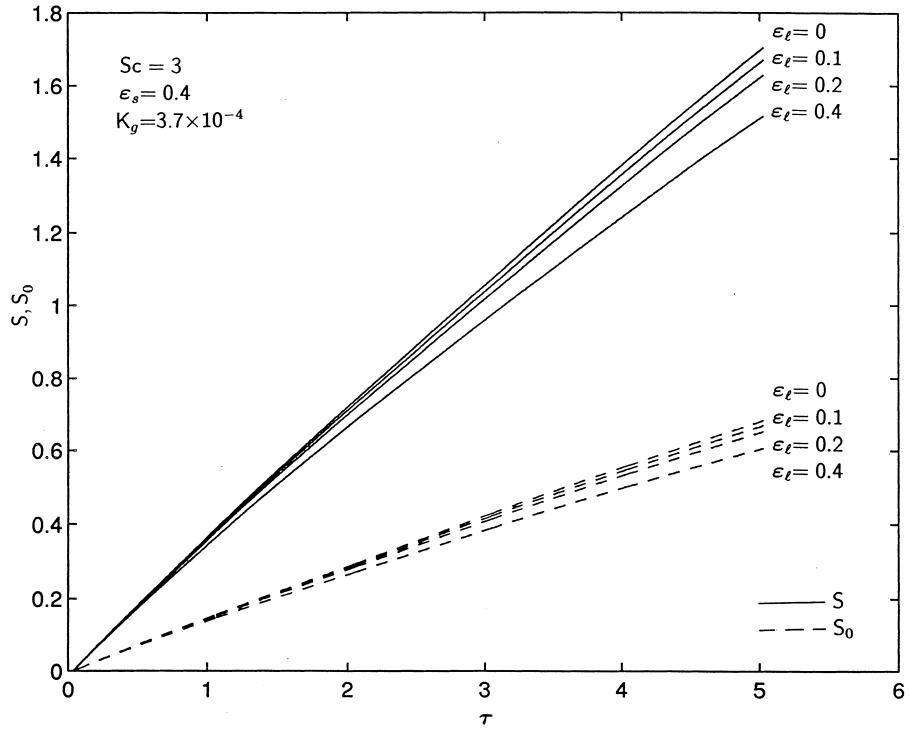

Fig. 5. Effect of porosity in the liquid phase on the locations of the liquid surface and the solid–liquid surface.

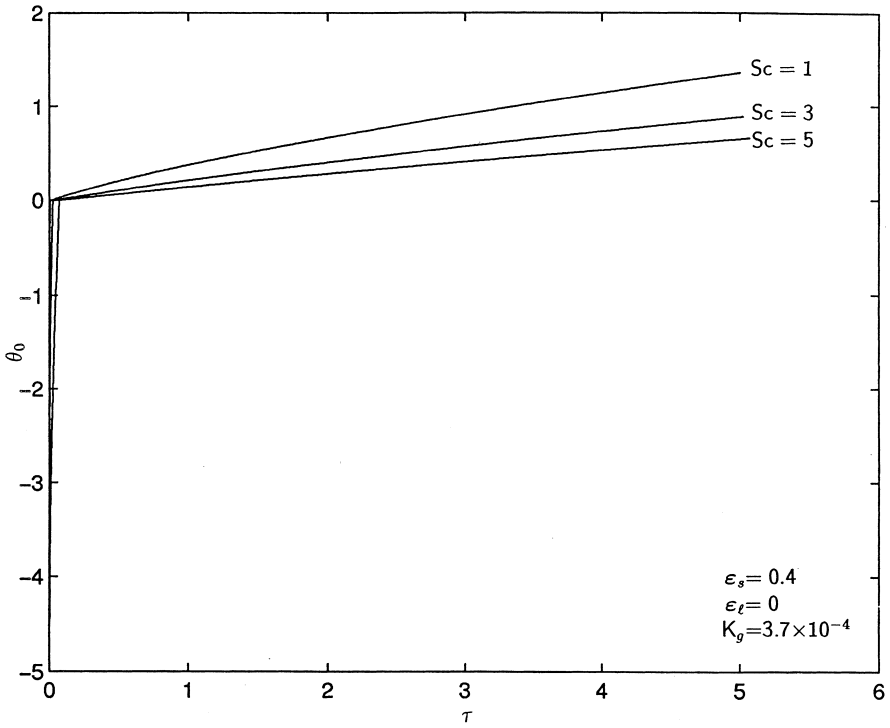

Fig. 6. Effect of subcooling on the surface temperature ($\varepsilon_s = 0.4$).

for different cases in Fig. 7. The effect of the initial subcooling of the powder bed on the surface temperature and the location of the interfaces at a different volume fraction of gas(es), $\varepsilon_s = 0.2$, are plotted in Figs 8 and 9. Compared with the cases of $\varepsilon_s = 0.4$, the duration of pre-heating is significantly increased because there are more particles needed to be heated for a lower volume fraction of gas(es). The other effects are, however, similar to the cases of $\varepsilon_s = 0.4$.

The effective thermal conductivity of the powder bed depends on the dimensionless thermal conductivity of the gas(es) filled in the powder bed. By analyzing a typical sintering system (Al–Fe), the value of dimensionless thermal conductivity of gas(es) was taken as $K_g = 3.7 \times 10^{-4}$. The effects of dimensionless thermal conductivity of the gas(es) on the surface temperature and the solid–liquid interface are plotted in Figs 10 and 11. It can be seen that the duration of pre-heating is slightly increased when the thermal conductivity of the gas(es) is increased to $K_g = 3.7 \times 10^{-3}$. The increase of thermal conductivity of the gas(es) will slow down the melting process. However, as can be seen in Figs 10 and 11, the effect of the dimensionless thermal conductivity of gas(es) on the melting process is very significant.

6. Conclusion

Melting of a powder mixture under constant heat flux heating is investigated analytically. Effect of density change of the powder bed during the melting process, which is very important for SLS, is modeled by considering the variation of the volume fraction of gas(es) in the powder bed during the melting process. By non-dimensionalizing the governing equations, the parameters of such a complicated process are reduced to four basic non-dimensional parameters: porosity of solid phase, volume fraction of gas(es) in liquid phase, initial subcooling parameter and dimensionless thermal conductivity of gas(es). Scale analysis shows that velocity induced by the density change must be taken into account. When shrinkage is not taken into account, the existence of the volume fraction of gas(es) in the powder bed increases both surface temperature and the velocity of the solid–liquid interface. However, at fixed solid phase porosity, shrinkage phenomenon accelerates the melting process and decreases the surface temperature. The initial subcooling of the powder bed decelerates the melting process and decreases the surface temperatures. The

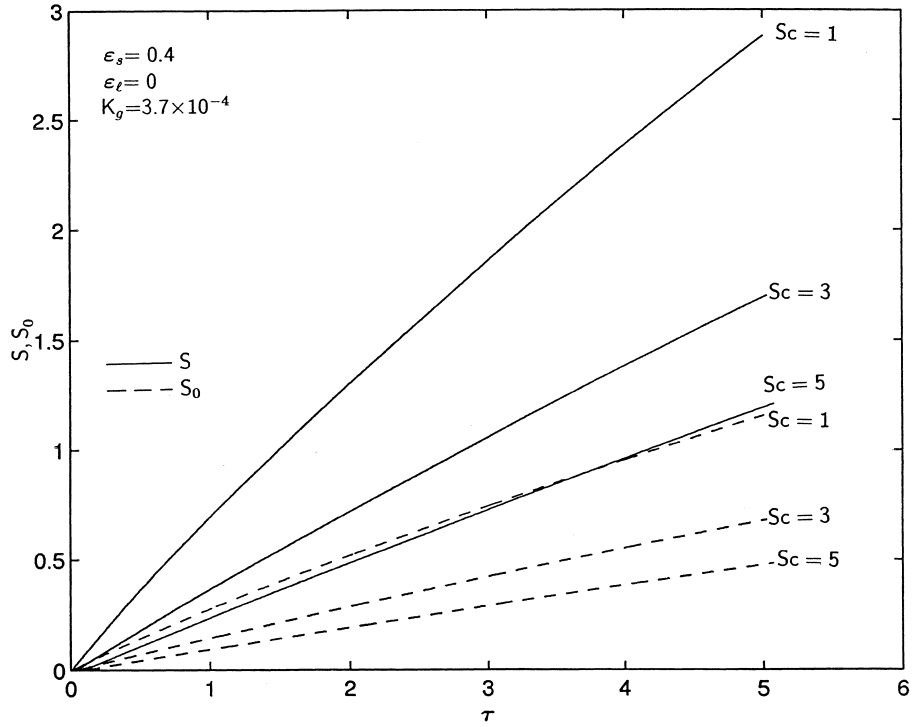

Fig. 7. Effect of subcooling on the locations of the liquid surface and the solid–liquid interface ($\varepsilon_s = 0.4$).

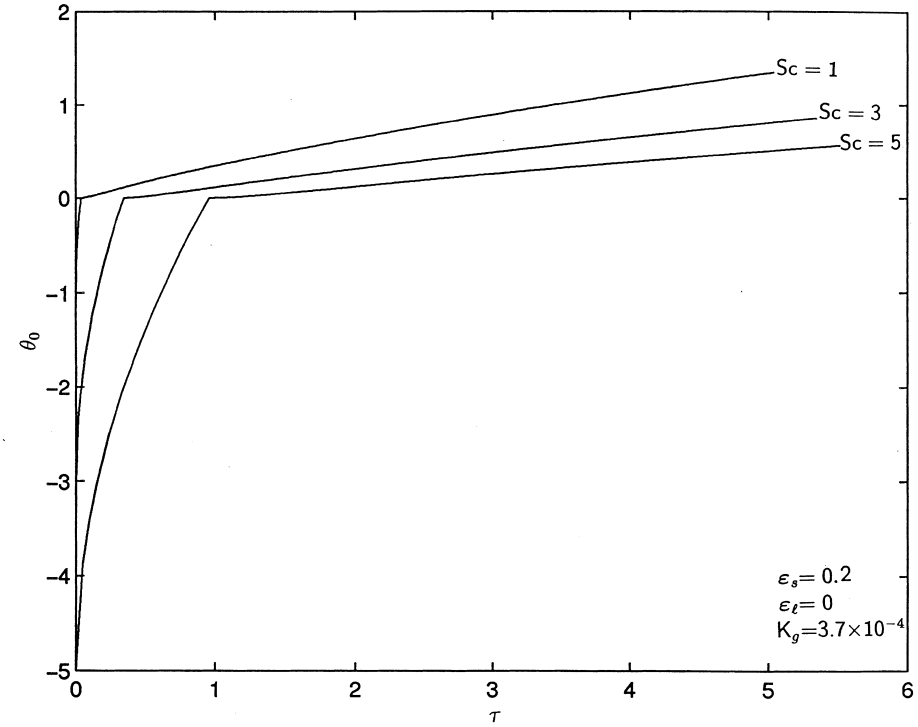

Fig. 8. Effect of subcooling on the surface temperature ($\varepsilon_s = 0.2$).

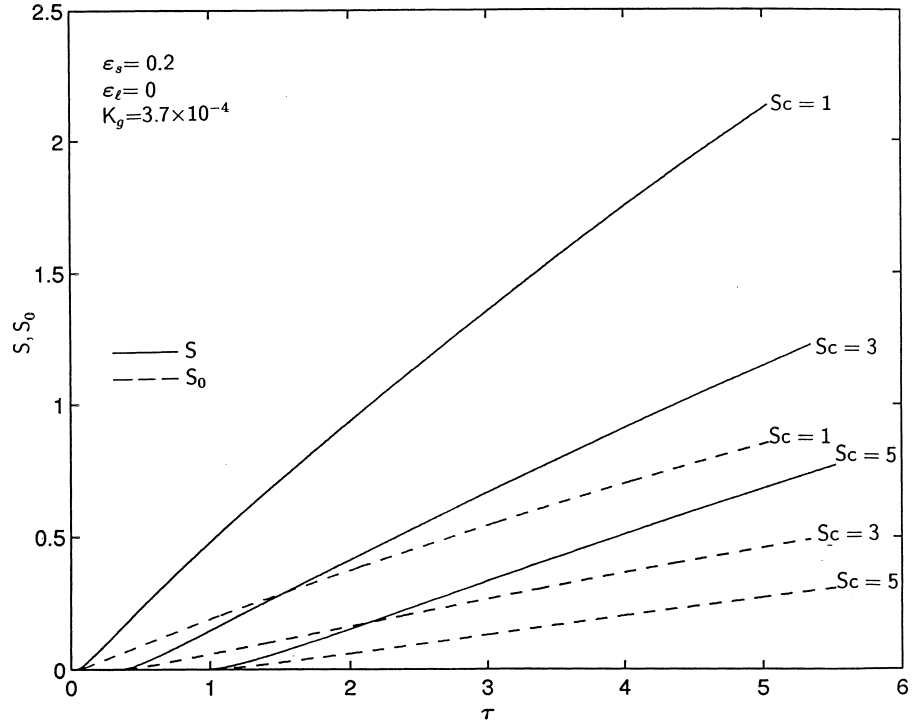

Fig. 9. Effect of subcooling on the locations of the liquid surface and the solid–liquid interface ($\varepsilon_s = 0.2$).

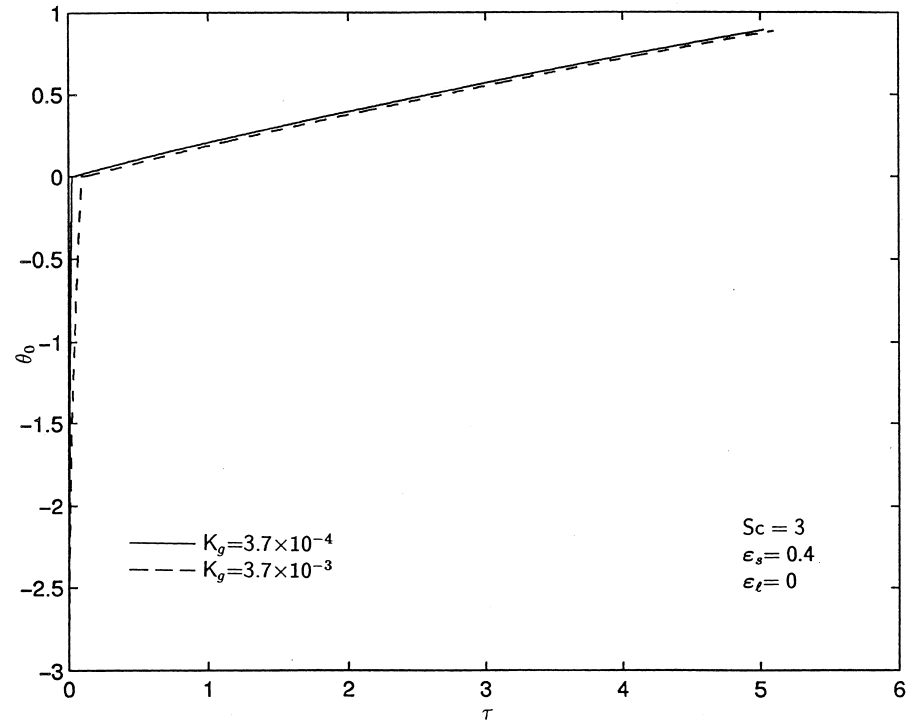

Fig. 10. Effect of dimensionless thermal conductivity of gas(es) on the surface temperature.

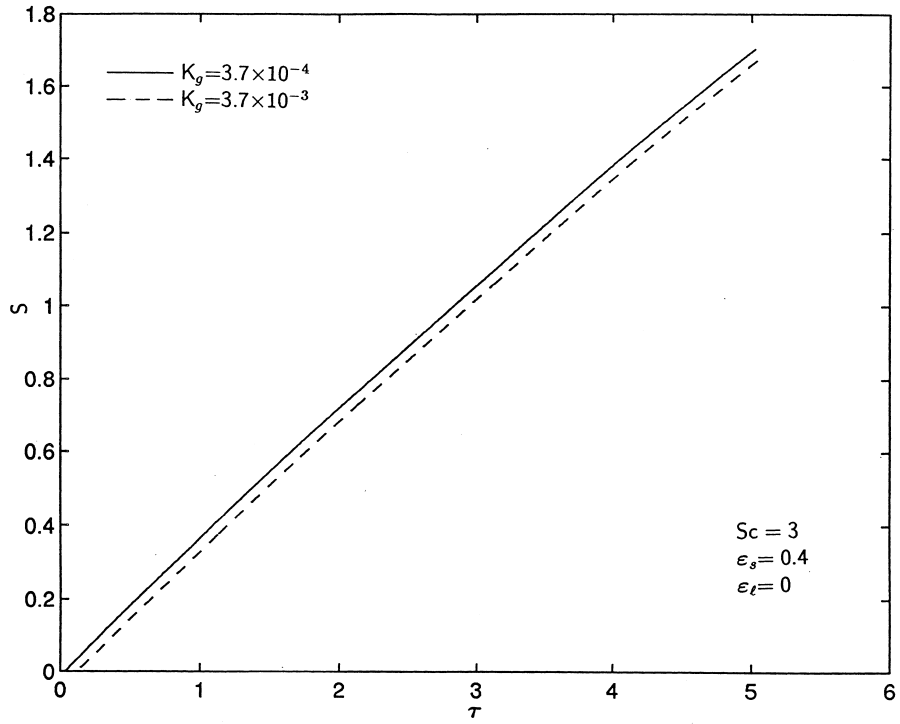

Fig. 11. Effect of dimensionless thermal conductivity of gas(es) on the solid–liquid interface.

physical model and results of this investigation paves the way to a simulation of the complicated 3-D SLS process.

References

[1] J.G. Conley, H.L. Marcus, Rapid prototyping and solid freeform fabrication, Journal of Manufacturing Science and Engineering 119 (1997) 811–816.
[2] M.M. Sun, J.J. Beaman, A three-dimensional model for selective laser sintering, Proceedings of Solid Freeform Fabrication Symposium 1995, pp. 102–109.
[3] J. Williams, D. Miller, C. Deckard, Selective laser sintering part strength as function of Andrew number, scan rate and spot size, Proceedings of Solid Freeform Fabrication Symposium 1996, pp. 549–557.
[4] M. Kandis, T.L. Bergman, Observation, prediction and correlation of geometric shape evolution induced by non-isothermal sintering of polymer powder, ASME Journal of Heat Transfer 119 (1997) 824–831.
[5] R. Viskanta, Phase change heat transfer, in: G.A. Lane (Ed.), Solar Heat Storage: Latent Heat Materials, CRC Press, Boca Raton, FL, 1983.
[6] L.C. Yao, J. Prusa, Melting and freezing, Advances in Heat Transfer 25 (1989) 1–96.
[7] E.R.G. Eckert, R.M. Drake, Analysis of Heat and Mass Transfer, McGraw-Hill, London, 1972.
[8] J. Crank, The Mathematics of Diffusion, Clarendon Press, Oxford, 1956.
[9] H.S. Carslaw, J.C. Jaeger, Conduction of Heat in Solids, Clarendon Press, Oxford, 1959.
[10] C. Charach, Y. Zarmi, Planar solidification in a finite slab: effect of density change, Journal of Applied Physics 70 (1991) 6687–6693.
[11] M. Conti, Planar solidification of a finite slab: effect of the pressure dependence of the freezing point, International Journal of Heat and Mass Transfer 38 (1995) 65–70.
[12] C.-J. Kim, S.T. Ro, Shrinkage formation during the solidification process in an open rectangular cavity, Journal of Heat Transfer 115 (1993) 1078–1081.
[13] A.A. Shah, Thermomechanical compressive melting of solder particles, M.S. thesis, University of Texas at Austin, 1994.
[14] T. Manzur, T. DeMaria, W. Chen, C. Roychoudhuri, Potential role of high power laser diode in manufacturing, presented at SPIE Photonics West Conference, San Jose, CA, 1996.
[15] D.E. Bunnell, Fundamentals of selective laser sintering of metals, Ph.D. thesis, University of Texas at Austin, 1995.
[16] M.P. Mughal, O.A. Plumb, Heat transfer during melting of packed particulate beds, in: D.A. Zumbrunnen et al. (Eds.), Heat and Mass Transfer in Materials Processing and Manufacturing, ASME HTD-Vol. 261 (1993) 63–72.

[17] M.P. Mughal, O.A. Plumb, Thermal densification of metal–ceramic composites, Scripta Metallurgica et Materialia 29 (1993) 383–388.
[18] G.R. Hadley, Thermal conductivity of packed metal powders, International Journal of Heat and Mass Transfer 29 (1986) 909–920.
[19] M.N. Ozisik, Heat Conduction, Wiley-Interscience, New York, 1980.
[20] Y.W. Zhang, Y.Y. Jin, Z.Q. Chen, Z.F. Dong, M.A. Ebadian, An analytical solution to melting in a finite slab with a boundary condition of the second kind, ASME Journal of Heat Transfer 115 (1993) 463–467.
[21] M.S. El-Genk, A.W. Cronenberg, Solidification in a semi-infinite region with boundary condition of the second kind: an exact solution. Letters in Heat and Mass Transfer 6 (1979) 321–327.